

A Robust Hybrid ACC-PM Approach for Personal Sound Zones

Yaqi Zhu¹, Lei Zhou¹, Hongqing Liu¹, Liming Shi¹, Lu Gan²

¹School of Communications and Information Engineering, Chongqing University of Posts and Telecommunications, Chongqing, China

²College of Engineering, Design and Physical Science, Brunel University, London UB8 3PH, U.K.

isyaqi.zhu@outlook.com, zhouleicqupt2016@outlook.com, hongqingliu@outlook.com, shilm@cqupt.edu.cn, lu.gan@brunel.ac.uk.

Abstract

The performance of personal sound systems is often degraded by inaccurate acoustic measurements. To achieve robust control while balancing acoustic contrast and signal distortion, this work proposes a robust hybrid optimization method that exploits both acoustic contrast control and pressure matching (ACC-PM). The method addresses perturbations caused by uncertainties in the acoustic transfer functions such as temperature changes, head movement, etc, modeled as norm-bounded uncertainties. Although the resulting worst-case optimization is inherently non-convex, it is reformulated as a second-order cone programming problem, which can be efficiently solved. Numerical simulations demonstrate the effectiveness of the proposed robust ACC-PM algorithm, showing an improvement over 18% in terms of AC compared to vanilla ACC-PM.

Index Terms: sound field control, worst-case, personal sound zone, second-order cone programming, robustness.

1. Introduction

Personal sound zones (PSZs) aim to create distinct auditory spaces where listeners can experience different sounds without physical barriers or wearing headsets [1]. With applications expanding in augmented/virtual reality (AR/VR), in-vehicle audio systems, and mobile devices, PSZ technology has gained significant attention in recent years. By utilizing loudspeaker arrays and tailored driving signals, PSZ systems generate bright zones (BZs), where desired sounds are heard, and dark zones (DZs), where sound energy is minimized, depicted in Figure 1. However, achieving this goal requires precise knowledge of acoustic transfer functions (ATFs) to optimize the sound pressure distribution between BZs and DZs. In practice, accurately capturing ATFs is challenging due to reverberation, mismatches in array positioning, listener movement, electro-acoustic variances, and unpredictable acoustic environments [2]. The traditional approaches designed with perfect ATFs may struggle or fail when faced with inaccuracies in the ATFs. Therefore, designing a robust PSZ control is highly desired in practical applications [3].

The conventional PSZ algorithms primarily focus on the optimizing criteria such as acoustic contrast (AC), acoustic contrast difference (AED) [4,5], reproduction error (RE), array effort (AE) [6], and planarity [7]. Choi and Kim introduced the well-known acoustic contrast control (ACC) in the frequency domain, while Elliott et al. rederived ACC using Lagrange multipliers and proposed regularized contrast maximization with an AE constraint, alongside a low-computation alternative maximizing AED [6]. However, ACC focuses on maximizing energy contrast, neglecting phase control, leading to audible distortions [8]. To address this, the pressure matching (PM) method [9] was

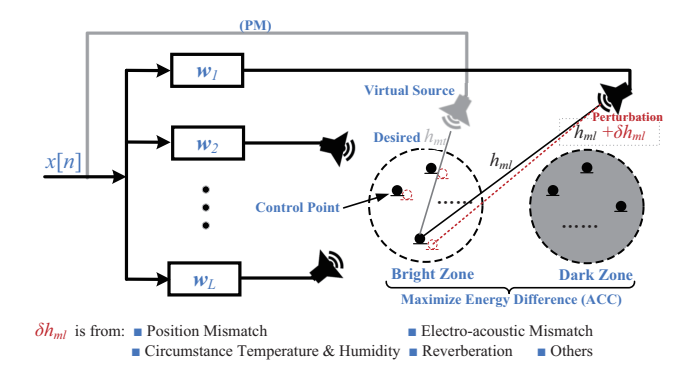


Figure 1: PSZ system schematic diagram and the potential factors causing ATFs' perturbation.

developed, which minimizes the reproduction error by considering both amplitude and phase at the cost of a lower AC. To balance ACC and PM, a hybrid approach through a trade-off weight was later proposed [10,11]. A subspace-based method, referred to as the variable span trade-off filters (VAST) [12], is also proposed based on generalized eigenvalue decomposition. In addition to the above frequency domain approaches, PSZ algorithm has also been extended to the time domain (TD) [8,13], the modal domain (MD) [14–16], and other transformed domains [17,18].

However, the aforementioned approaches usually assume perfect acoustic transfer functions (ATFs) to attain the required performance. A key consideration in robust PSZ control is linking the performance metrics to the uncertainty in ATFs. The existing robust PSZ methods can be broadly categorized into stochastic and robust optimization. In stochastic optimization, perturbations are treated as random variables following a known distribution such as additive or multiplicative errors in phase and amplitude [19, 20]. In contrast, robust optimization assumes norm-bounded uncertainties [21], using worst-case or min-max optimization approaches [6, 20, 22]. A hybrid approach [23] integrates both, using a complex Gaussian mixture model (CGMM) for parameter estimation and an uncertainty ellipsoid [24] to model perturbations. However, this method requires extensive ATF data and computations, with only moderate performance. Other studies focus on specific perturbations, such as position mismatch, temperature variations [25], or source geometry [26].

This paper proposes a robust ACC-PM (RACC-PM) algorithm based on worst-case optimization, utilizing norm-bounded uncertainty to alleviate ATF perturbations. The proposed RACC-PM is derived under more stringent assumptions than RACC while offering lower computational costs relative

to RPM. Additionally, the proposed method is formulated as a SOCP problem, which is solved via convex optimization [27].

2. Sound Zone Modeling and Preliminary

2.1. Sound Field Model and ATF Perturbation

We consider a two-zone PSZ system, controlled by L loud-speakers and sampled by M_B and M_D control points in BZ and DZ, respectively, shown in Figure 1. At the m-th control point in sound zone Z (BZ or DZ), denoted by the subscript $(\cdot)_{Z\in\{\mathrm{B,D}\}}$, the produced sound pressure $p_{mZ}[k]$ at the k-th frequency bin is

$$p_{mZ}[k] = x[k] \sum_{l=1}^{L} h_{ml,Z}[k] w_l[k] = x[k] \mathbf{h}_{mZ}^{\mathsf{T}}[k] \mathbf{w}[k], \quad (1)$$

where x[k] is the input signal, $w_l[k]$ is the driving signal for the l-th loudspeaker, and the ATF $h_{ml,Z}[k]$ denotes the acoustic environment between the m-th control point and the l-th loudspeaker in zone Z. Writing $\mathbf{h}_{mZ}[k] = [h_{m1,Z}[k], h_{m2,Z}[k], \cdots, h_{mL,Z}[k]]^{\mathrm{T}} \in \mathbb{C}^{L \times 1}$ and $\mathbf{w}[k] = [w_1[k], w_2[k], \cdots, w_L[k]]^{\mathrm{T}} \in \mathbb{C}^{L \times 1}$, the sound pressure $p_{mZ}[k]$ can be rewritten in vector form, and to account for the total sound pressure discretized by the microphone array, the sound field in zone Z can be compactly expressed in matrix form as

$$\mathbf{p}_{Z}[k] = x[k]\mathbf{H}_{Z}[k]\mathbf{w}[k], \tag{2}$$

where $\mathbf{H}_Z[k] = [\mathbf{h}_{1Z}[k], \cdots, \mathbf{h}_{M_Z Z}[k]]^T \in \mathbb{C}^{M_Z \times L}$ is premeasured ATF matrix, and $\mathbf{p}_Z[k] = [p_{1Z}[k], \cdots, p_{M_Z Z}[k]] \in \mathbb{C}^{M_Z \times 1}$ denotes the sound pressure vector. Assume x[k] is independent of $\mathbf{H}_Z[k]$ and $\mathbf{w}[k]$, it can be assumed to be a Dirac function. By omitting the frequency indices, a common expression for the sound field is [4-6,10]

$$\mathbf{p}_Z = \mathbf{H}_Z \mathbf{w}. \tag{3}$$

For ATFs with bounded perturbation, the measured ATFs can be denoted as

$$\tilde{\mathbf{H}}_Z = \mathbf{H}_Z + \Delta \mathbf{H}_Z, \ \|\Delta \mathbf{H}_Z\|_{\mathrm{F}} \le \epsilon_Z, \tag{4}$$

where $\Delta \mathbf{H}_Z$ represents the perturbation of the nominal measurement \mathbf{H}_Z , ϵ_Z is the uncertainty level, and $\|\cdot\|_{\mathrm{F}}$ denotes the Frobenius norm.

2.2. Evaluation Criteria

The performance of a PSZ system is primarily evaluated based on the following three key metrics: the ratio of sound pressure energy between BZ and DZ, the distortion error w.r.t. the desired sound field, and the power consumption of the loudspeakers. These metrics are quantified as acoustic contrast (AC), normalized reproduction error (NRE), and array effort (AE), respectively. The definitions of these metrics are

$$AC = 10 \log_{10} \frac{M_D \mathbf{w}^H \mathbf{H}_B^H \mathbf{H}_B \mathbf{w}}{M_B \mathbf{w}^H \mathbf{H}_D^H \mathbf{H}_D \mathbf{w}}, \quad AE = \frac{\mathbf{w}^H \mathbf{w}}{E_{ref}}, \quad (5)$$

and the NRE for both sound zones is defined as:

$$NRE = 10 \log_{10} \left(\frac{\|\mathbf{p}_{B}^{d} - \mathbf{H}_{B} \mathbf{w}\|^{2}}{\|\mathbf{p}_{B}^{d}\|^{2}} + \frac{\|\mathbf{H}_{D} \mathbf{w}\|^{2}}{\|\mathbf{p}_{B}^{d}\|^{2}} \right), \quad (6)$$

where E_{ref} is reference energy [6], and \mathbf{p}_{d}^{d} denotes the desired BZ sound field, while the desired sound field for DZ is $\mathbf{0}$. Typically, \mathbf{p}_{d}^{d} is designed in an anechoic environment, produced by

a virtual source [10, 28, 29], or simulated using a room impulse response (RIR) generator [30], which is then truncated to the direct path [12]. This operation indirectly allows PSZ to perform room compensation.

3. The Proposed Robust ACC-PM Using Worst-Case Optimization

The proposed robust RACC-PM seeks to mitigate the computational complexity issue of the robust PM (RPM) [23] and the unrealistic assumption of uncorrelated nominal measurements and perturbations in RACC [20]. RPM incurs additional costs due to the need for autocorrelation matrix estimation, which requires numerous ATF measurements. Furthermore, RPM does not account for perturbations in the DZ, and the biconvex nature of the optimization problem [31] leads to many local minima, where the commonly used alternating update approach cannot guarantee an optimal solution. Before deriving the RACC-PM algorithm, we introduce Theorem 1.

Theorem 1. For the following optimization, we have

$$\max_{\|\Delta \mathbf{H}\|_{\mathbf{F}} \le \epsilon} \|\mathbf{p} - (\mathbf{H} + \Delta \mathbf{H})\mathbf{w}\|_{2} = \|\mathbf{p} - \mathbf{H}\mathbf{w}\|_{2} + \epsilon \|\mathbf{w}\|_{2}.$$
(7)

Moreover, using the spectral norm or the Frobenius norm to measure the perturbation $\Delta \mathbf{H}$ yields the same result.

This can be easily proved using the triangle inequality and the definitions of the matrix norms. We omitted the proof here due to space constraints.

3.1. The Proposed Robust ACC-PM

To leverage both ACC and PM, we intuitively merge their cost functions and impose an ATF uncertainty constraint. Based on the worst-case principle, the worst-case RACC-PM formulation is

$$\begin{aligned} & \underset{\mathbf{w}}{\operatorname{min}} \underset{\Delta \mathbf{H}_{Z}}{\operatorname{mz}} \left\| \mathbf{p}_{\mathrm{B}}^{\mathrm{d}} - \tilde{\mathbf{H}}_{\mathrm{B}} \mathbf{w} \right\|_{2}^{2} + \mu \left\| \tilde{\mathbf{H}}_{\mathrm{D}} \mathbf{w} \right\|_{2}^{2} - \rho \left(\frac{\mathbf{w}^{\mathrm{H}} \tilde{\mathbf{R}}_{\mathrm{B}} \mathbf{w}}{\mathbf{w}^{\mathrm{H}} \tilde{\mathbf{R}}_{\mathrm{D}} \mathbf{w}} \right) \\ & \text{s.t.} \quad \left\| \mathbf{w} \right\|^{2} \leq e_{w}, \| \Delta \mathbf{H}_{\mathrm{B}} \|_{\mathrm{F}} \leq \epsilon_{B}, \| \Delta \mathbf{H}_{\mathrm{D}} \|_{\mathrm{F}} \leq \epsilon_{D}, \end{aligned} \tag{8}$$

where $\rho>0$ balances PM and ACC, and $\bar{\mathbf{R}}_Z$ denotes the correlation matrix of perturbed ATFs in the corresponding personal zone.

To solve this optimization in (8), the denominator is transformed as follows

$$\min_{\mathbf{w}} \max_{\Delta \mathbf{H}_{\mathrm{B}}, \Delta \mathbf{H}_{\mathrm{D}}} \|\mathbf{p}_{\mathrm{B}}^{\mathrm{d}} - \tilde{\mathbf{H}}_{\mathrm{B}} \mathbf{w}\|_{2}^{2} + \mu \|\tilde{\mathbf{H}}_{\mathrm{D}} \mathbf{w}\|_{2}^{2}
- \rho(\mathbf{w}^{\mathrm{H}} \tilde{\mathbf{R}}_{\mathrm{B}} \mathbf{w} - \alpha \mathbf{w}^{\mathrm{H}} \tilde{\mathbf{R}}_{\mathrm{D}} \mathbf{w}),$$
s.t.
$$\|\Delta \mathbf{H}_{\mathrm{B}}\|_{\mathrm{F}} \leq \epsilon_{B}, \|\Delta \mathbf{H}_{\mathrm{D}}\|_{\mathrm{F}} \leq \epsilon_{D}, \|\mathbf{w}\|^{2} \leq e_{w},$$

$$(9)$$

where α is a user-defined penalty parameter. Assuming $\tilde{\mathbf{R}}_{B} \succeq \alpha \tilde{\mathbf{R}}_{D}$, the last term in (9) exactly represents AED maximization [5].

Expanding the first two terms of ℓ_2 -norm in (9) produces

$$\min_{\mathbf{w}} \max_{\Delta \mathbf{H}_{B}, \Delta \mathbf{H}_{D}} \|\mathbf{p}_{B}^{d}\|_{2}^{2} - \mathbf{w}^{H} \tilde{\mathbf{H}}_{B}^{H} \mathbf{p}_{B}^{d} - \mathbf{p}_{B}^{d}^{H} \tilde{\mathbf{H}}_{B} \mathbf{w} + (1 - \rho) \mathbf{w}^{H} \tilde{\mathbf{R}}_{B} \mathbf{w} + (\mu + \rho \alpha) \mathbf{w}^{H} \tilde{\mathbf{R}}_{D} \mathbf{w}, \quad (10)$$
s.t.
$$\|\Delta \mathbf{H}_{B}\|_{F} \leq \epsilon_{B}, \|\Delta \mathbf{H}_{D}\|_{F} \leq \epsilon_{D}, \|\mathbf{w}\|^{2} \leq e_{w}.$$

Regrouping (10) yields

$$\min_{\mathbf{w}} \max_{\Delta \mathbf{H}_{B}, \Delta \mathbf{H}_{D}} (1 - \rho) \left\| \frac{1}{1 - \rho} \mathbf{p}_{B}^{d} - \tilde{\mathbf{H}}_{B} \mathbf{w} \right\|_{2}^{2} + (\mu + \rho \alpha) \left\| \tilde{\mathbf{H}}_{D} \mathbf{w} \right\|_{2}^{2} - \frac{\rho \sigma_{d}^{2}}{1 - \rho}, \tag{11}$$

s.t.
$$\|\Delta \mathbf{H}_{\mathrm{B}}\|_{\mathrm{F}} \leq \epsilon_{B}, \|\Delta \mathbf{H}_{\mathrm{D}}\|_{\mathrm{F}} \leq \epsilon_{D}, \|\mathbf{w}\|^{2} \leq e_{w},$$

where $\sigma_d^2 = \|\mathbf{p}_B^d\|_2^2$ represents the energy of desired sound pressure. Since the predefined parameters are constants independent of variables, the simplified expression of (11) becomes

$$\min_{\mathbf{w}} \max_{\Delta \mathbf{H}_{\mathrm{B}}, \Delta \mathbf{H}_{\mathrm{D}}} \left\| \frac{1}{1 - \rho} \mathbf{p}_{\mathrm{B}}^{\mathrm{d}} - \tilde{\mathbf{H}}_{\mathrm{B}} \mathbf{w} \right\|_{2}^{2} + \beta \left\| \tilde{\mathbf{H}}_{\mathrm{D}} \mathbf{w} \right\|_{2}^{2},
\text{s.t.} \quad \|\Delta \mathbf{H}_{\mathrm{B}}\|_{\mathrm{F}} \leq \epsilon_{B}, \|\Delta \mathbf{H}_{\mathrm{D}}\|_{\mathrm{F}} \leq \epsilon_{D}, \|\mathbf{w}\|^{2} \leq e_{w},$$
(12)

where $\beta = \frac{\mu + \rho \alpha}{1 - \rho}$. Using **Theorem 1**, we arrive at the final RACC-PM formulation. That is

$$\min_{\|\mathbf{w}\|^2 \le e_w} \left\| \begin{bmatrix} \mathbf{p}_{\mathrm{B}}^{\mathrm{d}} - \sqrt{1 - \rho} \mathbf{H}_{\mathrm{B}} \\ \mathbf{0} - \sqrt{\mu + \rho \alpha} \mathbf{H}_{\mathrm{D}} \end{bmatrix} \mathbf{w} \right\|_{2} + \epsilon_r \|\mathbf{w}\|_{2}, \quad (13)$$

where $\epsilon_r = \sqrt{(1-\rho)\epsilon_B^2 + (\mu+\rho\alpha)\epsilon_D^2}$. It is seen that introducing the AC constraint reshapes the nominal measurements in effect.

3.2. Solutions of RACC-PM

To solve the problem in (13), which consists of a quadratic objective function and a quadratic constraint, we reformulate (13) as an SOCP problem by introducing auxiliary variables λ and ν , given by

min
$$\lambda$$

s.t. $\|\mathbf{p} - \mathbf{H}\mathbf{w}\|_{2} \le \lambda - \nu$,
 $\|\mathbf{w}\|_{2} \le \frac{\nu}{\epsilon_{r}}$,
 $\|\mathbf{w}\|_{2} \le \sqrt{e_{w}}$, (14)

where $\mathbf{p} = \left[\mathbf{p}_{\mathrm{B}}^{\mathrm{d}^{\mathrm{T}}}, \mathbf{0}^{\mathrm{T}}\right]^{\mathrm{T}} \in \mathbb{C}^{(M_{B}+M_{D})\times 1}$ and $\mathbf{H} = \left[\sqrt{1-\rho}\mathbf{H}_{\mathrm{B}}^{\mathrm{T}}, \sqrt{\mu+\rho\alpha}\mathbf{H}_{\mathrm{D}}^{\mathrm{T}}\right]^{\mathrm{T}} \in \mathbb{C}^{(M_{B}+M_{D})\times L}$. For computational convenience, we define the complex desired sound field and driven signal as

$$\mathbf{y} = \begin{bmatrix} \operatorname{Re}(\mathbf{p}) \\ \operatorname{Im}(\mathbf{p}) \end{bmatrix}, \ \mathbf{x} = \begin{bmatrix} \operatorname{Re}(\mathbf{w}) \\ \operatorname{Im}(\mathbf{w}) \end{bmatrix}.$$
 (15)

To preserve the product $(\mathbf{H}\mathbf{w})$, we define the measurement ATFs matrix \mathbf{A} as:

$$\mathbf{A}^{(2M_B + 2M_D) \times 2L} = \begin{bmatrix} \operatorname{Re}(\mathbf{H}) & -\operatorname{Im}(\mathbf{H}) \\ \operatorname{Im}(\mathbf{H}) & \operatorname{Re}(\mathbf{H}) \end{bmatrix}. \tag{16}$$

Using the definitions in (15) and (16), we reformulate (14) as a general SOCP problem, given by

min
$$\mathbf{c}^{\mathrm{T}}\mathbf{z}$$

s.t. $\|\mathbf{C}_{i}\mathbf{z} + \mathbf{d}_{i}\|_{2} \leq \mathbf{e}_{i}^{\mathrm{T}}\mathbf{z} + f_{i}, \quad i = 1, 2, 3,$ (17)

where $\mathbf{z} = [\mathbf{x}^{\mathrm{T}}, \lambda, \nu]^{\mathrm{T}} \in \mathbb{R}^{2L+2}$ and $\mathbf{c} = [\mathbf{0}^{\mathrm{T}}, 1, 0]^{\mathrm{T}} \in \mathbb{R}^{2L+2}$. The matrices and vectors used in the constraints are provided in Table 1.

Finally, the problem in (13) can be efficiently solved using the convex optimization toolbox [27]. The computation

Table 1: Constant References.

Variables	Index	1	2	3
$\mathbf{C}_{i}^{(2M_B+2M_I)}$	$)\times(2L+2)$	$[\mathbf{A},0]$	$[\mathbf{I}, 0]$	$[\mathbf{I}, 0]$
$\mathbf{d}_{i}^{(2M_{B}+2M_{B})}$		$-\mathbf{y}$	0	0
$\mathbf{e}_i^{(2L+2) imes 1} \qquad \qquad \left[0^{\mathrm{T}}, 1, -1 ight]^{\mathrm{T}} \ \left[0^{\mathrm{T}}, 0, rac{1}{\epsilon_r} ight]^{\mathrm{T}} \ 0$			$[\cdot]^{\mathrm{T}}$ 0	
f_i		0	0	$\sqrt{e_w}$

complexity of RACC-PM is $\mathcal{O}(8M_BL^2+8M_DL^2+8L^3)$ for each iteration [32] with the interior-point primal-dual potential reduction method. In comparison, CGMM, using the interior-point polynomial algorithm, has a complexity of $\mathcal{O}(8M_B^3L^3+8L^3)$ [33, pp. 236].

4. Numerical Experiment

This section presents numerical experiments to validate the effectiveness of the proposed RACC-PM. We compare the proposed RACC-PM with several benchmarks: robust worst-case ACC (wc-RACC) [20], ACC-PM [10], narrowband VAST (VAST-NF) [12], and POTDC-RACC [34]. The robustness of these algorithms is evaluated against perturbations in ATFs, with disturbed ATFs generated using the RIR toolbox [30]. The analysis is conducted across three scenarios: the presence of background noise, different reverberation times, and mismatched microphone array positions.

4.1. Experiment Settings

The room dimensions are set to $4.5m \times 4.5m \times 2.5m$ (length \times width \times height), with the layout of the equipment shown in Figure 2.

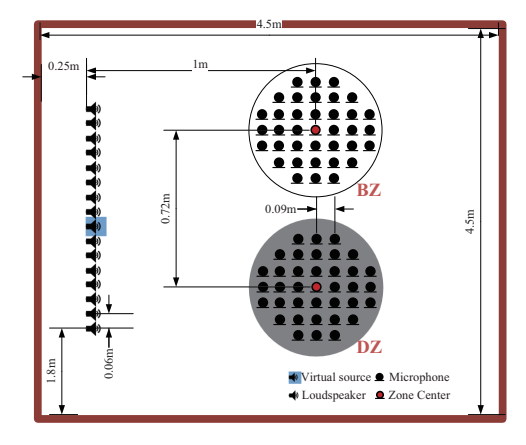


Figure 2: Room Setup: A linear array of 16 (L = 16) uniformly spaced loudspeakers and two sets of 37 measurement microphones $(M_B = M_D = 37)$ with equal spacing between each. A virtual source generates the desired sound field.

In the experiments, we synthesized 300 sets of ATF data under three perturbation scenarios. In **Case 1**, 100 sets were subjected to random Gaussian noise interference, which represents the background noise in the room, with an SNR ranging from 15 dB to 25 dB. In **Case 2**, 100 sets were contaminated by disturbances in microphone positions, where the microphones were uniformly distributed within a circular area of 0.05 m ra-

dius around their true positions. Finally, in **Case 3**, 100 sets were affected by disturbances at reverberation time T_{60} , uniformly sampled between 300 and 400 ms. The parameters for all algorithms are provided in Table 2.

Table 2: Parameters Setting.

Algorithms	Parameters	
ACC(True)/PM(True)	<u> </u>	
ACC-PM	$\kappa = 0.7.$	
VAST-NF	$\mu = 1, V = L/2 = 8$.	
wc-RACC	$\gamma_{ m B}pprox\epsilon_B^2, \gamma_{ m D}pprox\epsilon_D^2.$	
POTDC-RACC	α_l, α_u [34], $\eta = \epsilon_B$,	
	$\gamma_{\rm D}=\gamma_{\rm D}$ in wc-RACC.	
RACC-PM	$\sqrt{e_w} = \ \mathbf{w}_{\text{ACC-PM}}\ , \mu = 1,$	
	$\alpha = AC_{ACC(True)}, \rho = 0.1,$	
	$\epsilon_B = 0.01 \sqrt{\text{tr}(\mathbf{H}_B^H \mathbf{H}_B)},$	
	$\epsilon_D = 0.01 \sqrt{\text{tr}(\mathbf{H}_{\mathrm{D}}^{\mathrm{H}} \mathbf{H}_{\mathrm{D}})}.$	

4.2. Evaluation Results

The performance comparisons of all algorithms in terms of NRE, AC, and AE are shown in Figure 3 and 4. The solid red line represents the proposed RACC-PM, while PM (True) and ACC (True) denote the best NRE and AC achieved under undisturbed conditions, respectively.

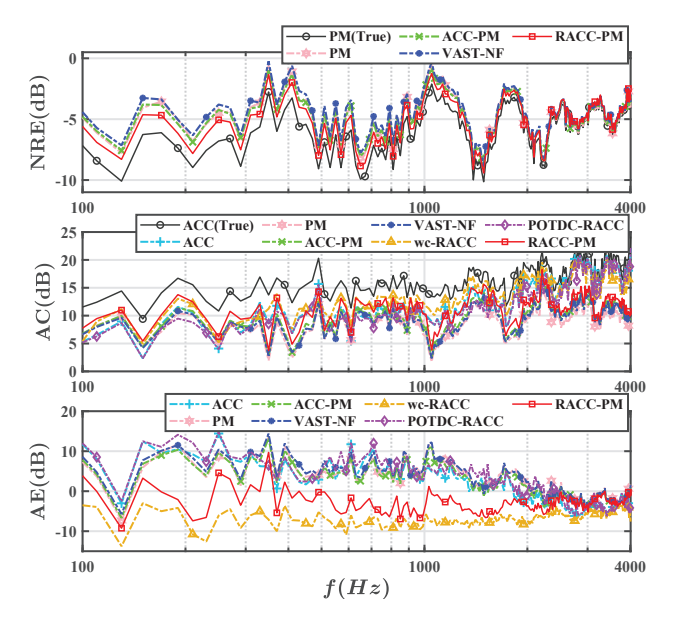


Figure 3: Case 1: Background noise.

For Case 1, involving 100 data sets, we used leave-one-out cross-validation, and the average results are shown in Figure 3. When nominal data are used, PM and ACC achieve the best performance for the NRE and AC metrics, respectively. However, both algorithms significantly deteriorate NRE and AC when applied to perturbed ATFs. The robust algorithms mitigate this issue, with wc-RACC yielding the best AC performance. Notably, the proposed RACC-PM algorithm matches the AC performance of wc-RACC in the 100–1000 Hz range while offering superior NRE performance. Additionally, RACC-PM

demonstrates comparable AE to wc-RACC, which is enhanced by incorporating an AE constraint.

In Case 2, position mismatch exerts a greater impact on both the AC and NRE metrics, with NRE degradation in the 1000–4000 Hz band being more pronounced than in Case 1. The proposed RACC-PM algorithm improves AC performance over non-robust methods while preventing further degradation of NRE, particularly in low-frequency bands below 1000 Hz. While POTDC-RACC, wc-RACC, and ACC achieve higher AC values than RACC-PM, they are primarily optimized for AC, with NRE remaining around 0 dB. In contrast, RACC-PM jointly optimizes AC and NRE, leading to more balanced and robust performance. Notably, compared to all baselines in Figure 4, RACC-PM achieves an average AE reduction of approximately 20 dB, significantly improving the acoustic radiation efficiency of the speaker array and highlighting its practical potential for real-world sound field control.

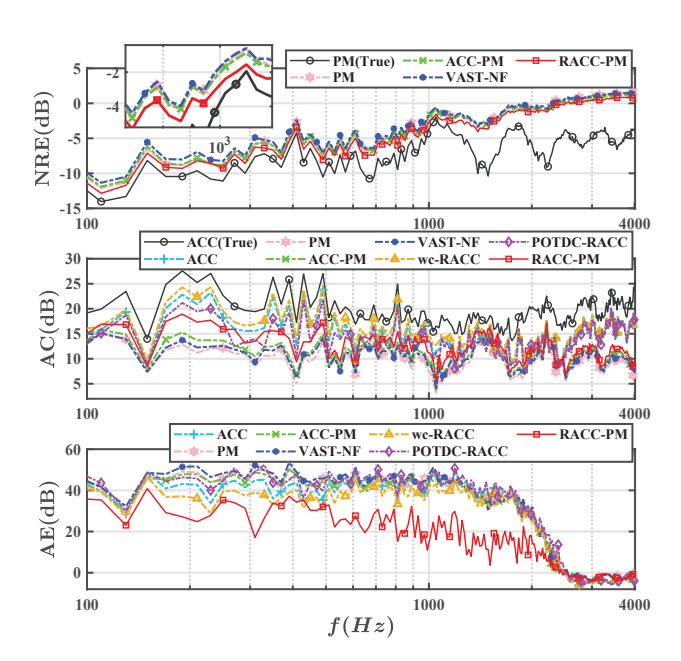


Figure 4: Case 2: Position mismatch.

The results of ${\bf Case~3}$ caused by reverberation are consistent with these observations, leading to a more pronounced performance degradation, and due to page limitations, the results are not presented here.

5. Conclusion and Discussion

In this work, we developed a new RACC-PM algorithm, derived from worst-case optimization, to address the mismatch between measured and nominal ATFs. Although the optimization is nonconvex, it can be reformulated as SOCP by imposing an AC constraint, allowing for efficient solutions via convex optimization. The effectiveness was demonstrated in a disturbed PSZ model under various perturbations, where it outperformed the standard ACC-PM. Currently, we are implementing RACC-PM in a real-world cabin environment to achieve PSZ between the front and rear seats. Our findings indicate that RACC-PM remains effective, even without diagonal loading.

6. References

- [1] W. Druyvesteyn and J. Garas, "Personal sound," *Journal of the Audio Engineering Society*, vol. 45, no. 9, pp. 685–701, 1997.
- [2] J.-Y. Park, J.-W. Choi, and Y.-H. Kim, "Acoustic contrast sensitivity to transfer function errors in the design of a personal audio system," *The Journal of the Acoustical Society of America*, vol. 134, no. 1, pp. EL112–EL118, 2013.
- [3] T. Betlehem, W. Zhang, M. A. Poletti, and T. D. Abhayapala, "Personal sound zones: Delivering interface-free audio to multiple listeners," *IEEE Signal Processing Magazine*, vol. 32, no. 2, pp. 81–91, 2015.
- [4] J.-W. Choi and Y.-H. Kim, "Generation of an acoustically bright zone with an illuminated region using multiple sources," *The Journal of the Acoustical Society of America*, vol. 111, no. 4, pp. 1695–1700, 2002.
- [5] M. Shin, S. Q. Lee, F. M. Fazi, P. A. Nelson, D. Kim, S. Wang, K. H. Park, and J. Seo, "Maximization of acoustic energy difference between two spaces," *The Journal of the Acoustical Society* of America, vol. 128, no. 1, pp. 121–131, 2010.
- [6] S. J. Elliott, J. Cheer, J.-W. Choi, and Y. Kim, "Robustness and regularization of personal audio systems," *IEEE Transactions on Audio, Speech, and Language Processing*, vol. 20, no. 7, pp. 2123–2133, 2012.
- [7] P. J. Jackson, F. Jacobsen, P. Coleman, and J. Abildgaard Pedersen, "Sound field planarity characterized by superdirective beamforming," in *Proceedings of Meetings on Acoustics*, vol. 19, no. 1. AIP Publishing, 2013.
- [8] Y. Cai, M. Wu, and J. Yang, "Design of a time-domain acoustic contrast control for broadband input signals in personal audio systems," in 2013 IEEE International Conference on Acoustics, Speech and Signal Processing. IEEE, 2013, pp. 341–345.
- [9] M. Poletti, "An investigation of 2-d multizone surround sound systems," in *Audio Engineering Society Convention 125*. Audio Engineering Society, 2008.
- [10] J.-H. Chang and F. Jacobsen, "Sound field control with a circular double-layer array of loudspeakers," *The Journal of the Acoustical Society of America*, vol. 131, no. 6, pp. 4518–4525, 2012.
- [11] M. B. Møller, M. Olsen, and F. Jacobsen, "A hybrid method combining synthesis of a sound field and control of acoustic contrast," in *Audio Engineering Society Convention* 132. Audio Engineering Society, 2012.
- [12] T. Lee, L. Shi, J. K. Nielsen, and M. G. Christensen, "Fast generation of sound zones using variable span trade-off filters in the dft-domain," *IEEE/ACM Transactions on Audio, Speech, and Language Processing*, vol. 29, pp. 363–378, 2020.
- [13] M. F. Simón Gálvez, S. J. Elliott, and J. Cheer, "Time domain optimization of filters used in a loudspeaker array for personal audio," *IEEE/ACM Transactions on Audio, Speech, and Language Processing*, vol. 23, no. 11, pp. 1869–1878, 2015.
- [14] W. Zhang, T. D. Abhayapala, T. Betlehem, and F. M. Fazi, "Analysis and control of multi-zone sound field reproduction using modal-domain approach," *The Journal of the Acoustical Society of America*, vol. 140, no. 3, pp. 2134–2144, 2016.
- [15] Q. Zhu, X. Qiu, P. Coleman, and I. Burnett, "A comparison between two modal domain methods for personal audio reproduction," *The Journal of the Acoustical Society of America*, vol. 147, no. 1, pp. 161–173, 2020.
- [16] W. Zhang, J. Zhang, T. D. Abhayapala, and L. Zhang, "2.5 d multizone reproduction using weighted mode matching," in 2018 IEEE International Conference on Acoustics, Speech and Signal Processing (ICASSP). IEEE, 2018, pp. 476–480.
- [17] N. Antonello, E. De Sena, M. Moonen, P. A. Naylor, and T. Van Waterschoot, "Room impulse response interpolation using a sparse spatio-temporal representation of the sound field," *IEEE/ACM Transactions on Audio, Speech, and Language Pro*cessing, vol. 25, no. 10, pp. 1929–1941, 2017.

- [18] M. Hahmann and E. Fernandez-Grande, "A convolutional plane wave model for sound field reconstruction," *The Journal of the Acoustical Society of America*, vol. 152, no. 5, pp. 3059–3068, 2022
- [19] Y. Cai, L. Liu, M. Wu, and J. Yang, "Robust time-domain acoustic contrast control design under uncertainties in the frequency response of the loudspeakers," in *INTER-NOISE and NOISE-CON Congress and Conference Proceedings*, vol. 249, no. 1. Institute of Noise Control Engineering, 2014, pp. 5775–5780.
- [20] Q. Zhu, P. Coleman, M. Wu, and J. Yang, "Robust acoustic contrast control with reduced in-situ measurement by acoustic modeling," *Journal of the Audio Engineering Society*, 2017.
- [21] S. J. Elliott, W. Jung, and J. Cheer, "Causality and robustness in the remote sensing of acoustic pressure, with application to local active sound control," in *ICASSP 2019-2019 IEEE Interna*tional Conference on Acoustics, Speech and Signal Processing (ICASSP). IEEE, 2019, pp. 8484–8488.
- [22] C. Daskalakis, S. Skoulakis, and M. Zampetakis, "The complexity of constrained min-max optimization," in *Proceedings of the 53rd Annual ACM SIGACT Symposium on Theory of Computing*, 2021, pp. 1466–1478.
- [23] J. Zhang, L. Shi, M. G. Christensen, W. Zhang, L. Zhang, and J. Chen, "CGMM-based sound zone generation using robust pressure matching with ATF perturbation constraints," *IEEE/ACM Transactions on Audio, Speech, and Language Processing*, 2023.
- [24] R. G. Lorenz and S. P. Boyd, "Robust minimum variance beamforming," *IEEE transactions on signal processing*, vol. 53, no. 5, pp. 1684–1696, 2005.
- [25] T. Betlehem, L. Krishnan, and P. Teal, "Temperature robust active-compensated sound field reproduction using impulse response shaping," in 2018 IEEE International Conference on Acoustics, Speech and Signal Processing (ICASSP). IEEE, 2018, pp. 481–495
- [26] S. A. Verburg, F. Elvander, T. van Waterschoot, and E. Fernandez-Grande, "Optimal sensor placement for the spatial reconstruction of sound fields," *EURASIP Journal on Audio, Speech, and Music Processing*, vol. 2024, no. 1, p. 41, 2024.
- [27] M. Grant and S. Boyd, "CVX: Matlab software for disciplined convex programming, version 2.1," https://cvxr.com/cvx, Mar. 2014
- [28] M. B. Mller, M. Olsen, and F. Jacobsen, "A hybrid method combining synthesis of a sound field and control of acoustic contrast," in *Audio Engineering Society Convention*, 2012.
- [29] M. Hu, H. Zou, J. Lu, and M. G. Christensen, "Maximizing the acoustic contrast with constrained reconstruction error under a generalized pressure matching framework in sound zone control," *The Journal of the Acoustical Society of America*, vol. 151, no. 4, pp. 2751–2759, 2022.
- [30] J. B. Allen and D. A. Berkley, "Image method for efficiently simulating small-room acoustics," *The Journal of the Acoustical So*ciety of America, vol. 65, no. 4, pp. 943–950, 1979.
- [31] J. Gorski, F. Pfeuffer, and K. Klamroth, "Biconvex sets and optimization with biconvex functions: a survey and extensions," *Mathematical methods of operations research*, vol. 66, no. 3, pp. 373–407, 2007.
- [32] L. Vandenberghe and S. Boyd, "Semidefinite programming," *SIAM review*, vol. 38, no. 1, pp. 49–95, 1996.
- [33] Y. Nesterov and A. Nemirovskii, Interior-point polynomial algorithms in convex programming. SIAM, 1994.
- [34] J. Zhang, L. Shi, M. G. Christensen, W. Zhang, L. Zhang, and J. Chen, "Robust acoustic contrast control with positive semidefinite constraint using iterative POTDC algorithm," in 2022 International Workshop on Acoustic Signal Enhancement (IWAENC). IEEE, 2022, pp. 1–5.